DEVELOPMENT STATUS OF TUF CODE

W.S. Liu, A. Tahir, E. Zaltsgendler, W. Kelly and R.K. Leung

Reactor Safety and Operational Analysis Department
Ontario Hydro Nuclear
700 University Avenue
Toronto, Ontario, M5G-1X6

ABSTRACT

An overview of the important development of the TUF code in 1995 is presented. The development in the following areas is presented: control of round-off error propagation, gas resolution and release models, and condensation induced water hammer. This development is mainly generated from station requests for operational support and code improvement.

1. TUF ACTIVITIES AND DEVELOPMENT AREAS

The reactor system codes, SOPHT and TUF, for the CANDU reactor stations in Ontario Hydro Nuclear are maintained and supported by the Reactor Safety and Operational Analysis Department (RSOAD). Most of the developmental activities related to thermal-hydraulics at RSOAD have been concentrated on the TUF code. Those activities are mainly generated from station requests for operational support and the code improvement. Close cooperation and liaison between RSOAD and all stations has been maintained. Further cooperation with other institutions (AECL, universities and other utilities) on thermal-hydraulic development of CANDU reactors is through COG (CANDU Owners Group) and user group meetings. The current RSOAD activities associated with the TUF code are: (1) providing training and support to users; (2) assuring to comply with quality assurance (QA) procedure for code and input data changes; (3) conducting code validation; and (4) continuing code development and improvement.

An issue that was raised by the regulatory authority (AECB) was the fact that TUF was not developed under a QA program. To satisfy this requirement, a QA team for TUF was set up. The major objectives of this QA team are (1) provide adequate documentation, (2) review of the coding with respect to the code specification document, (3) record and report code errors, perform impact assessment and notify all users, (4) assure coding changes follows the QA requirement, and (5) construct new versions of TUF. In additional to the QA team, a TUF users' supporting group has been set up to provide the technical support to analysts and to document all possible areas of code improvement. The development status of the TUF code was reported to all analysts during the users group meetings. This direct communication between the analysts and the code developers has significantly improved the code quality and predictions. For the plant simulations, a large responsibility has been imposed on the code user to prepare the proper input data. It can be fulfilled only if the user is fully aware of the physical modelling and the limitations of the codes. Therefore, user guidelines and training might be the easiest way to improve the quality of the code predictions. The preparation and testing of an input deck for a reactor is a tedious task which requires a clear quality assurance strategy to follow. The best way to reduce the user effect is to remove all the options by just using the best estimate model and to improve the code with respect to the physical modelling. The developmental activities are basically driven by two considerations: removing the code deficiencies and implementing the new models. In general, the code developments can be grouped in the following aspects: (1) numerical methods and computing efficiency, (2) physical modelling for all related modules, (3) sensitivity studies for important parameters, options and models, (4) update

of the controller systems for all stations, (5) cooperation with other component codes used in Ontario Hydro Nuclear, and (6) problems related to safety and operational support analyses.

After the report on the TUF development status in 1994 (Reference 1), a few areas relevant to the TUF development have been undertaken in 1995. These activities are grouped and summarized in the following areas: control of round-off error propagation, gas dissolved and release models, water hammer simulation, pump restart model, condensation heat transfer coefficient for a mixture of steam and non-condensible gas, and unification of the LOCA and water hammer versions. The first three topics are the main subject of this paper, that have been reported at the TUF users' group meetings.

In the development of reactor system analysis code, there are three programming areas which require special attention: the variations caused by the computer compiler, the accuracy of restart files and the round-off error inherent in the digital computers. Using the optimization option for the compiler, the results should be checked against those produced by other compiler options (for example the debug options). The restart files should include *all* necessary variables and common blocks used in the program. The transient solutions should be independent of the timing when the restart files are produced. The round-off error has not received special attention in most system analysis codes. In reality, it may significantly affect the accuracy of transient solutions, depending on the order of matrix equations and the type of computing machine used. There are two particular concerns in the study of round-off error: accuracy of solutions and its propagation during the transient. The last concern is the first subject discussed in this paper. The coolant in the primary and secondary heat transport systems of a CANDU reactor may contain dissolved gas. Under transient conditions, the dissolved gas may be released when its concentration is higher than the saturated or equilibrium concentration. As a result, it may affect the water level measurement (for example in the bleed condenser) during operation. Dissolved gas in the reactor piping and components may be a problem but it has not received proper attention either in analysis or experiment. It is hoped that further research work on this particular area will be conducted in the Canadian research institutes. A simplified engineering model has been developed for the TUF code to simulate the behaviour of gas content release and resolution processes. A brief description of the modelling of gas content is the second subject of this paper. As shown in Reference 1, TUF has the capability to simulate the condensation induced water hammer phenomenon. Currently, two approaches have been adopted for this problem in the TUF development plan: the injection front model and the distinct regions model. The main physics behind both approaches is the last subject of this paper.

2. CONTROL OF ROUND-OFF ERROR PROPAGATION

There are two fundamental sources of error in solving the initial value problem: truncation (or formula) error and round-off error. For example, consider the following initial value problem:

$$\frac{\partial x}{\partial t} = f(t, x), \quad x(t_0) = x_0 \qquad [1]$$

by a numerical procedure such as the first-order implicit method:

$$x_{n+1} = x_n + \frac{\delta t\, f(t_n, x_n)}{1 - \frac{\partial f}{\partial x}\delta t}, \quad t_n = t_0 + n\,\delta t \qquad [2]$$

where δt is the time step size. The difference between the exact solution $x(t_n)$ and the approximate solution x_n

$$E_n = x(t_n) - x_n \qquad [3]$$

is the truncation error. The round-off error R_n is defined as

$$R_n = x_n - X_n \qquad [4]$$

where X_n is the value actually computed by the given numerical procedure. The absolute value of the total error is given by

$$| x(t_n) - X_n | \leq | E_n | + | R_n | \qquad [5]$$

The round-off error depends on the type of computing machine used and the sequence in which the computations are carried out. Round-off errors stem from a finite number of digits in a computer word, while truncation errors are due mainly to finite approximations of limiting processes. When a decimal number which contains a fractional part is converted to its binary equivalent, a conversion error due to the finite word length of the computer may be introduced. Another source of round off error may be introduced if the calculation requires more digits than available through a machine or compiler. The study of round-off errors and the control of their propagation is important in high-speed digital computations. In some cases, it may be needed to estimate the final round-off made in solving a given problem by a specific numerical method. The propagation of the round-off error may become a problem for a circuit with symmetric piping or branches since the error can be amplified as the transient progresses. The symmetric behaviour of the flow matrix equations will be destroyed. In this work, the technique to control the round-off error propagation in the TUF code is described. It should be noted that the solution accuracy is not the main concern in this technique.

Iterative Technique

In all thermal-hydraulic codes, the direct method for solving a system of linear equations has been employed. In this method, round-off errors at each time step of the calculations are usually carried to the next time step if they have not been controlled. If the equation number is quite large such as that for a reactor circuit simulated in the safety analysis, these errors grow as the calculations progress, and considerable care must be exercised to prevent them nullifying the transient solutions. In this case, the iterative techniques possess a certain advantage in that the round-off error of one iteration tends to be corrected in subsequent iteration. For example, consider the following system of linear equation

$$A\,x = B \qquad [6]$$

by any one of the elimination algorithms. Assuming that some round-off errors are present in the k^{th} iterative solution x_k, the error vector e_k is defined as

$$e_k = x - x_k \qquad [7]$$

and the residual vector r_k be defined by

$$r_k = B - A\,x_k \qquad [8]$$

If the system of equations

$$A\,\delta_k = r_k \qquad [9]$$

could be solved exactly, the solution

$$x_{k+1} = x_k + \delta_k \qquad [10]$$

would solve the original system A x = B exactly. The iterative improvement algorithm may be terminated when δk is sufficiently small.

This technique with one iteration has been tested in the TUF code to simulate the case with five identical inner zones (each having 28 channels) in the broken passes of Bruce A circuit for a 40% RIH break, where the HT pumps are credited in the simulation. It has been concluded that the round-off error is generally less serious in the iterative technique than it is for direct methods. However, the computation time has increased considerably (about 30%) and the propagation of the round-off error still exists as the transient progresses. As shown in Figure 1, the sheath temperatures of the top pin at the centre of the five identical channels are different from each other after transient time 50 seconds. As a result, the iterative technique for the matrix solver was abandoned from the computing economic point of view.

Technique with Different Precision Levels

Rounding errors can often be eliminated by carrying one, two, or even more extra figures, known as guarding figures, in the intermediate steps of calculation. To control the round-off error propagation in the transient solutions, several techniques have been exercised in the steady state and transient programs. The causes for non-symmetric results in the identical channels have been identified in the following areas: (1) in the do-loop process of the summations of the following equations: (A + B) + C , and A + (B + C), where A and B are relatively large and C is relatively small; and (2) in the process of the matrix inversion and solutions. The number of extra figures theoretically needed, according to the analysis of von Neumann (Reference 2) gets to be almost prohibitive for the inversion of a matrix of the order of 100 or so. However, there is some indication that many of the matrices met in practice are better behaved than those admitted in the analysis. A simple approach was adopted in the code. The higher precision (for example, double precision) than that used for the rest (for example, single precision) of the calculations has been utilized in these two particular areas. Using this technique with different precision levels for the variables, the round-off error has been controlled. This error has not propagated to the next time step. As a result, the simulation of five identical channels in the reactor circuit has shown that all identical channels have identical results over a long transient period. As shown in Figure 2, the sheath temperatures at the centre of the five identical channels are identical. Also the combination of using the quadruple and the double precision has been tested in the program. The symmetric behaviour of all identical channels has also been preserved, even though the computation time has increased considerably (more than double). It confirms that the technique implemented in the code can indeed eliminate the propagation of round-off errors.

The identical channels have been arranged in the following configurations in the network of Bruce A circuit: (1) sequentially grouped together in the critical pass, (2) four identical channels located at the end of the PHT modules, and (3) four identical channels located at the end of the circuit modules. The main purpose of these input arrangements was to check the effect of channel locations in the flow matrix equations. It has shown that identical results have been obtained for these different network arrangements. It also confirms the technique used in the control of round-off error propagation in the matrix equations.

3. GAS RELEASE AND RESOLUTION MODELS

Most liquids contain dissolved gases in solution, although the volumetric proportion may be very small. Dissolved gases and gas bubbles in liquids provide nucleation points and assist in the onset of cavitation. Under transient conditions, the dissolved gas may be released (so-called desorption or stripping) when the concentration of the dissolved gas is higher than the saturated (or equilibrium) concentration. This is the so-called gaseous cavitation. Also, when the local liquid pressure falls below the vapour pressure or during the vapour generation process (or

liquid flashing), the dissolved gas will be released. This phenomenon is termed vaporous cavitation. Vaporous cavitation takes place almost instantly while gaseous cavitation is a much slower process. Extensive cavitation can produce unacceptable noise levels. On the other hand, resolution of gas (or absorption) in liquid will occur, even at a much slow rate, when the content concentration is below the equilibrium value. The decision whether to account for gas release during a pressure transient depends upon the extent of gas dissolved and the low pressure residence times. For example, the transient pressures may exist below the gas saturation pressure for extended times in the case of cold water injection. If the content of dissolved gas is greater than the equilibrium value, significant gas release will take place and should be considered in order to correctly simulate the transient (Reference 3). The other example where the gas may release during the pressure transient is the water hammer phenomenon. The effects of vaporous cavitation on the fluid transient have been extensively studied in the simulation of water hammer. In this work, emphasis is placed on the engineering model rather than on the detailed physical processes of bubble growth and collapse.

To simulate the gas release and resolution in the reactor circuit, several physical aspects should be considered: (1) the transport equation for dissolved gas content, (2) the release and dissolved rates, (3) the conservation equations for the gas phase, and (4) the equations of state for a mixture of two components, where the component water may contain liquid and vapour. The last two items have already been considered in TUF and will not be discussed here. The first two items are the subjects discussed here.

Transport Equation for Dissolved Gas Content

The three-dimensional transport equations for multi-component systems relating to gas-liquid mass transfer and chemical reaction have been proposed by some authors (for example Reference 4). Similar to the one-dimensional thermal-hydraulic equations, the one-dimensional transport equations for multi-component systems can be obtained by using the cross-sectional average process. As a result, the final one-dimensional transport equations are identical to those used in thermal-hydraulics, except the mass transfer model. In the vapour-liquid system, the phase change rate results from the interfacial heat transfer rate, while in the gas-liquid system the mass transfer rate results from the molecular diffusion process. Similar to the interfacial heat transfer process for the vapour-liquid system, the main driving force for the mass transfer process in the gas-liquid system is the difference between the intrinsic phase concentration and the concentration at the interface. Normally, the interfacial concentration is assumed equal to the equilibrium concentration.

To simplify the physical model, the dissolved gas in the liquid is considered as a part of the homogeneous liquid mixture with equal temperatures and velocities since the amount of gas content considered is small in the current applications. Define a mass fraction for the dissolved gas as c:

$$c = \frac{M_c}{M_f} \qquad [11]$$

where M_c is the total mass of the dissolved gas content and M_f is the total liquid mass including the dissolved gas content in a control volume. The mass conservation equations for all the components are listed in Table 1. The notations M and W denote the mass and flow rate, respectively. F denotes the production rate. The subscript f is for liquid including gas content, l for pure liquid, c for gas content, a for non-condensable gas, g for vapour, eva for evapouration, cond for condensation and mw for metal-water reaction. The transport equation for the dissolved gas content can be written as

$$M_f \frac{dc}{dt} = \sum_{in} (c_{in} - c) W_{f,in} - c F_{eva} - F_a \qquad [12]$$

where W_f is the liquid flow rate, F_{eva} is the vapour generation rate and F_a is the total gas release or dissolved rate due to the concentration gradient between the intrinsic phase concentration and the interfacial value within the

control volume. The vapour generation rate has been described in the two-fluid model implemented in TUF; its formulation will not be discussed here. In this paper, only two physical parameters are described: the gas release and resolution models and the equilibrium concentration of gas content. Since the gas content is treated as a part of the liquid phase, the transport equation for the dissolved gas content can be solved explicitly in the code. To eliminate the possible numerical diffusion, the tracing of the concentration front in a control volume during the content injection period has been performed in the code.

Gas Release and Resolution Models

Gas release and resolution are a diffusion controlled process of interfacial mass transfer. The concentration gradient is the main driving force in this process. In the gas release model (gas content concentration is higher than the equilibrium value), the following simple form analogous to the interfacial heat transfer is assumed:

$$F_a = V A_i H_c (C - C_i) \qquad [13]$$

where V is the control volume, A_i is the effective interfacial area per unit volume, H_c is the interfacial mass transfer coefficient for gas content, C is the content concentration in solution in kg/m^3, and C_i is the concentration at interface which is function of pressure and temperature. The relationship between C and c is given by

$$C = \frac{c M_f}{V} \qquad [14]$$

Substituting Equation [14] into Equation [13], the gas release rate becomes

$$F_a = \frac{M_f}{\tau_c} (c - c_i), \quad c > c_i \qquad [15]$$

where τ_c is the so-called relaxation times for gas release which are defined as

$$\tau_c = \frac{1}{A_i H_c} \qquad [16]$$

As discussed in Reference 5, the relaxation time for gas release in a mixed flow regime is about 1 s. It is expected that the time constant t_c are between 1 second and 1000 seconds, depending on the flow regimes. This value should be determined from experimental data.

In a steady state, the gas content in a control volume can be calculated from Equation [12] as follows:

$$c = \frac{c_{in} W_f + \frac{M_f}{\tau_c} c_{sat}}{W_f + F_{eva} + \frac{M_f}{\tau_c}} \qquad [17]$$

It shows that for a subcooled liquid ($F_{eva}=0$) in a control volume without inflows, the gas content should not exceed the equilibrium gas content. For the case where the gas content is below its equilibrium value and there is no gas available for absroption, the local gas content is calculated from the following equation:

$$c = \frac{\sum_{in} c\, W_f}{\sum_{in} W_f} \qquad [18]$$

Equilibrium Concentration of the Dissolved Gas

The mass of dissolved gas in a volume of liquid is given by Henry's law when the fluid is in an equilibrium state. The concentration of dissolved gas in a solvent is directly proportional to the partial pressure of the gas when temperature remains constant. The proportionality constant in Henry' law is known as the solubility coefficient, or the Bunsen absorption coefficient. The mole fraction solubility x is expressed by

$$x = \frac{p}{k} \qquad [19]$$

where p is the partial pressure of the gas, and k is the Henry's law constant for the gas at a given temperature. By the definition, the mole fraction solubility is expressed by

$$x = \frac{n(a)}{n(a) + n(f)} \qquad [20a]$$

where n(a) is the number of gas moles in the volume and n(f) is the number of fluid moles. For slightly soluble gases like air in water, the mole fraction solubility is approximately expressed by

$$x \sim \frac{n(a)}{n(f)} \qquad [20b]$$

From experimental data, Henry's law holds quite well when the partial pressure of soluble gas is less than 101 kPa. For the case with a partial pressure of soluble gas greater than 101 kPa, the constant k is seldom independent of the partial pressure of the soluble gas. For the CANDU reactor, the air content in D_2O and H_2O is of concern. There are few experimental data available for solubility in the light and heavy water over a wide range of pressure up to 10 MPa and temperature up to 310 C. But the experimental data and some correlations for solubilities of the air components, nitrogen and oxygen, are available in the literature. From Equation [20], the solubility of air can be expressed by

$$x_a = x_N + x_O \qquad [21]$$

where x_a, x_N and x_O are the mole fraction of air, nitrogen and oxygen, respectively. As shown in Reference 5, the following correlations for equilibrium concentration of nitrogen in light water are suggested:

$T < 350$ K

$$\ln x = -67.3966 + 86.32129\,\frac{1}{\tau} + 24.79808 \ln \tau + 0.952105 \ln p - 0.000477\, p \qquad [22]$$

$T > 350$ K

where t=T[K]/100 and p is pressure in bar. Figure 3 shows the pressure dependence of the equilibrium concentration of nitrogen in light water.

$$\ln x = -43.0160 + 48.5244 \frac{1}{\tau} + 13.9321 \ln \tau + 0.97004 \ln p - 0.000483 p \qquad [23]$$

The solubility of oxygen in light water has probably been the most intensively studied gas solubility system. The following correlations for solubility of oxygen as a function of pressure and temperature are recommended:

$T < 373$ K

$$\ln x = -3.7236 - 55.9617 \frac{1}{\tau} + 104.9668 \frac{1}{\tau^2} + 1.033 \ln p - 0.00574 p \qquad [24]$$

$T > 373$ K

$$\ln x = 4.1796 - 131.04 \frac{1}{\tau} + 341.7 \frac{1}{\tau^2} - 247.49 \frac{1}{\tau^3} + 1.033 \ln p - 0.00574 p \qquad [25]$$

Figure 4 illustrates the pressure dependence of the equilibrium concentration of oxygen in light water. It should be noted that the pressure in Equations [22] to [25] is the partial pressure of the gas. Therefore, we have $p = 0.8\ p_a$ for Equations [22] and [23], and $p = 0.2\ p_a$ for Equations [24] and [25], where p_a is the air pressure.

Little research has been done on the solubility of gases in heavy water. Cosgove and Walkley (Reference 6) have reported the solubility of nitrogen in D_2O for a narrow range of temperature ($T < 313$ K) at a nitrogen partial pressure of 101 kPa. The measured mole fraction is about 7% - 10% higher in D_2O than that in H_2O. But due to lack of experimental data for wide range of temperature and pressure, it is assume that the mole fraction solubilities in D_2O are the same as that in H_2O for engineering applications.

The equilibrium concentration for air c_{sat} which is needed to solve Equation [15] can be found from the mole fraction solubility by using the definition c from Equation [11]. Taking into account that $M_f = n_f m_f$, one can obtain

$$c_{sat} = x_a \frac{m_a}{m_f} \qquad [26]$$

where m_a and m_f are the molecular weights of air and fluid.

Gas Content in Reactors

The standard procedure to ensure the low level of air or other non-condensible gases in the reactor heat transport systems is to vent the system during fill up, and to carry out draw-down operations. At present, it is not known how much gas is released during the normal operating conditions and what is the exact gas content in the system. The degree of uncertainty of this problem is large. The gas content in the heat transport system strongly depends on the original content, amount of hydrogen added, and the history of gas venting and unit operation.

The sources of the non-condensible gases in the reactor circuit mainly result from the original soluble air in coolant and from the radiolysis of D_2O under the influence of radiation to produce D_2 and O_2 gases. Usually, the O_2 concentration is reduced by removing ionic and soluble impurities through the ion exchanger columns in the heat transport purification system (similar manner as done in the moderator purification system). To further reduce the O_2 concentration (to reduce corrosion and radiolysis rate), hydrogen or deuterium gas is added to the system at high pressure. The purpose of inserting hydrogen gas is to scavenge the oxygen and recombine with it forming water.

The main concerns for the effects of gas content on the reactor thermal-hydraulics are in the following areas: (1) water level measurements in system components bleed condenser, pressurizer and water tank when the pressures drop to below their corresponding equilibrium values; (2) capability of heat removal of heat exchangers when the mass fraction of released gas is not small; and (3) the effect of released gas on the ECI performance.

3. CONDENSATION INDUCED WATER HAMMER

During the past years, a series of tests for condensation induced water hammer has been conducted at Ontario Hydro Technologies (OHT). The main purpose of these tests was to examine the induced pressure pulses under various defined flow conditions and to define the threshold condition between the water hammer and no water hammer regions. The complexity of the tests was held to a minimum and the dominant physical parameters were accurately measured. The TUF code was chosen to simulate these tests since it was used in the simulation of the emergency cooling system of the steam generators. Therefore, these tests were used to examine the condensation model and the numerical method applied in the TUF code. The setup for the tests consisted of a vertical tank filled with sub-cooled water (the schematic diagram of the OHT apparatus was shown in Reference 1). The air supply system at the top of the tank was used to maintain a constant tank pressure during the transient. A horizontal pipe (length 5.5 m and diameter 0.0921 m) initially filled with sub-cooled water was connected from the bottom of the tank. A fast-acting ball valve was installed between this pipe and a closed-end vertical pipe (length 5 m and diameter 0.0921 m) initially filled with steam. Pressure transducers were mounted in the vertical pipe to record the pressure history of the experiment. A series of tests with different tank pressures, water temperatures and steam temperature was performed. The following results have been observed: The magnitudes of the induced pressure pulses are functions of the tank pressure, the water temperature and the steam temperature. There is a threshold condition between the water hammer and no water hammer regions. Finally, a scatter of the test data with the same test conditions was observed.

After the results presented in Reference 1, the condensation induced water hammer has been further examined in the past year in order to explain the possible physics for the scatter of the test data observed in OHT water hammer tests. Two approaches have been adopted for this particular problem in the TUF development plan. One still uses the injection front model in the simulation, as described in Reference 1. This model is currently used in the code for general applications. In this model, the averaged condensation rate over the steam filled pipe is used in the two-fluid model. The other approach is based on the physics observed from the OHT test data. Different models are used in three observed distinct regions: valve induced dispersion front, adiabatic region and fast condensation zone. The physics behind both approaches are the main subjects described here. The second approach is currently being tested in the code. Further development is required before it is utilized. Also, it should be noted that the main objective of a reactor system code is to predict the averaged system response rather than a detailed local response under a particular condition. Therefore, the second approach is only used for this particular problem. Its extension to a general case and its effect on the overall thermal-hydraulics require further consideration. Nevertheless, the physics behind both approaches are discussed below.

Injection Front Model

In this model, the valve opening is assumed to be in a condition that the injection front has a distinct interface before it collides with the pipe dead-end. Also, certain entrained bubbles and droplets caused by the movement of the interface are assumed to exist at the interface. The interfacial area per unit volume A_i consists of three components: injection front, entrained bubbles, and entrained droplets

$$A_i = \frac{1}{L} + \frac{6\,\Delta\alpha_b}{D_b} + \frac{6\,\Delta\alpha_d}{D_d} \qquad [27]$$

where L is the pipe length, D_b is the bubble diameter, D_d is the droplet diameter, $\Delta\alpha_b$ is the void fraction of the entrained bubbles in the liquid region, and $\Delta\alpha_d$ is the void fraction of the entrained droplets in the vapour region.

The phase transfer rate is mainly controlled by the liquid phase.

The interfacial heat transfer coefficients for the distinct interface, and the entrained bubbles and droplets are given by

$$H_{gi} = \max [H_{gi}(conv) , H_{gi}(cond)] \quad [28]$$

$$H_{fi} = \max [H_{fi}(conv) , H_{fi}(cond)]$$

For the distinct interface, the convective and conductive heat transfer coefficient are given by

$$H_{ki}(conv) = 0.023 \frac{K_k}{D_{pipe}} Re_k^{0.8} Pr_k^{0.4} \quad [29]$$

$$H_{ki}(cond) = Nu \frac{K_k}{D_{pipe}}$$

and for the entrained particles, they are given by

$$H_{ki}(conv) = 2 \frac{K_k}{D_{pipe}} [1 + 0.37 Re_k^{0.5} Pr_k^{0.33}] \quad [30]$$

$$H_{ki}(cond) = Nu \frac{K_k}{D_p}$$

where the subscript k stands for phase g (gas) or f (liquid), K_k is the phase thermal conductivity, D_{pipe} is the pipe diameter, D_p is the particle diameter, Re_k and Pr_k are the Reynolds and Prandtl numbers for phase k, respectively, and Nu is the Nusselt number (4.132 for laminar and 16.134 for turbulent flow). The phase slip velocity is used in the evaluation of the phase Reynolds number.

In this model, two cases are simulated: (1) the most severest case with a tank pressure 654 kPa, water temperature 23 C and steam temperature 150 C (it caused a damage at the closed end piping), and (2) tank pressure 551 kPa, water temperature 22 C and steam temperature 142 C. The predicted result of the pressure transient at the dead-end location for Case (1) is shown in Figure 5. The corresponding test data are plotted in Figure 6. The results for Case (2) are plotted in Figures 7 and 8, respectively. It shows that waterhammer phenomenon is well predicted by this model. However, the magitudes of pressure spikes at the dead-end location for Case (2) are over-predicted. Also, the pressure transient before the first pressure spike does not reflect the transient behaviour observed in the tests since the average condensation rate over the steam filled pipe was used in this model.

Distinct Regions Model

In order to explain the reasons for data scatter in the OHT water hammer tests, the whole set of the test data has been re-examined, especially in the pressure transients before the first pressure spike at the pipe dead-end. It has been found that three distinct regions in the pressure transient have been observed as shown in Figure 9 for Case 2: initial

valve induced flow dispersion, slow condensation and fast condensation regions.

In this model, it is assumed that the valve opening results in a regime of liquid dispersion which is similar to that observed in the jet injection with a cloud of droplets. In this region, a large condensation rate is obtained due to the large value of the interfacial area. After the supplied steam flow in the injection node (induced by condensation) forces the droplets to settle down to its water level, a perfect distinct interface (without entrainments) is assumed in the second region. The condensation rate is so low such that the steam compression process is close to the adiabatic condition. At the end of compression process, an instability at the interface occurs which results in drastic changes in the flow regime and the condensation mode (from film condensation to drop-wise condensation). As a result, the condensation rate is so large such that the steam pressure drops significantly before the void collapses at the pipe dead-end.

This distinct regions model was hypothesized from the observation of the test results. There are several difficulties in implementing this model in the reactor system code. (1) The tracing of the jet position in the discrete grid is required. (2) The interaction between the droplets with the steam flow is required. (3) The interfacial instability criterion from the adiabatic region to the fast condensation region is difficult to obtain theoretically. (4) This particular model may not be applicable to other flow conditions, for example in the case of a horizontal pipe. Nevertheless, an attempt to model this test has been made even though some difficulties still exist. The details of this modelling will be presented elsewhere. Figure 10 shows the predicted pressure transient at the pipe dead-end for Case 2, where the initial pressure transient before the first pressure peak is well predicted.

5. CONCLUDING REMARKS

A general description on the development of the TUF code in 1995 has been presented. The applications of the gas release and resolution models on certain system components are being tested. The generalization of the distinct regions model to other flow conditions and piping geometries, for example in a vertical downward flow and in a horizontal pipe, is being planned.

ACKNOWLEDGEMENT

The coordination and assistance provided by E. Mistele between RSOAD and OHT, and the experimental data received from Dr. A. Chan at OHT for the water hammer experiment are acknowledged.

REFERENCES

1. W.S. Liu and R. Leung, TUF Development Status and Applications, 15th Annual Conference of Canadian Nuclear Society, June 5-8, 1994, Montreal, Quebec, Canada.

2. J. von Neumann and H.H. Goldstine, Numerical inverting of matrixes of high order, Bull. Am. Math. Soc. 53, pp.1021, 1947.

3. D.C. Wiggert and M.J. Sundquist, The Effect of Gaseous Cavitation on Fluid Transient, J. Fluids Eng., 101, March 1979.

4. S. Whitaker, The transport equations for multi-phase systems, Chem. Engng. Sci., 28, p.139, 1973.

5. E. Zaltsgendler, W.S. Liu and R.K. Leung, Gas resolution and released models in reactor thermal-hydraulics, CNS Simulation Symposium, Oct. 15-17, 1995, McMaster University, Hamilton, Ontario, Canada.

6. B.A. Cosgrove and J. Walkley, Solubility of gases in H2O and D2O, J. Chromatogr., 216, p. 161, 1981.

Table 1.

Mass conservations of various components of a control volume

Components	Mass Conservation Equations
Pure liquid and gas content	$\frac{dM_f}{dt} = \sum_{in} W_f - \sum_{out} W_f - F_{eva} + F_{cond} - F_a$ $M_f = M_l + M_c, \quad W_f = W_l + W_c$
Pure liquid	$\frac{dM_l}{dt} = \sum_{in} W_l - \sum_{out} W_l - (1-c)\, F_{eva} + F_{cond}$ $M_l = (1-c)\, M_f, \quad W_l = (1-c)\, W_f$
Gas content	$\frac{dM_c}{dt} = \sum_{in} W_c - \sum_{out} W_c - c\, F_{eva} - F_a$ $M_c = c\, M_f, \quad W_c = c\, W_f$
Non-condensable gas phase	$\frac{dM_a}{dt} = \sum_{in} W_a - \sum_{out} W_a + F_a + c\, F_{eva} + F_{mw}$
Vapour phase	$\frac{dM_g}{dt} = \sum_{in} W_g - \sum_{out} W_g + (1-c)\, F_{eva} - F_{cond} - F_{mw}$
Total mixture	$\frac{dM}{dt} = \sum_{in} W - \sum_{out} W$ $M = M_f + M_a + M_g, \quad W = W_f + W_a + W_g$

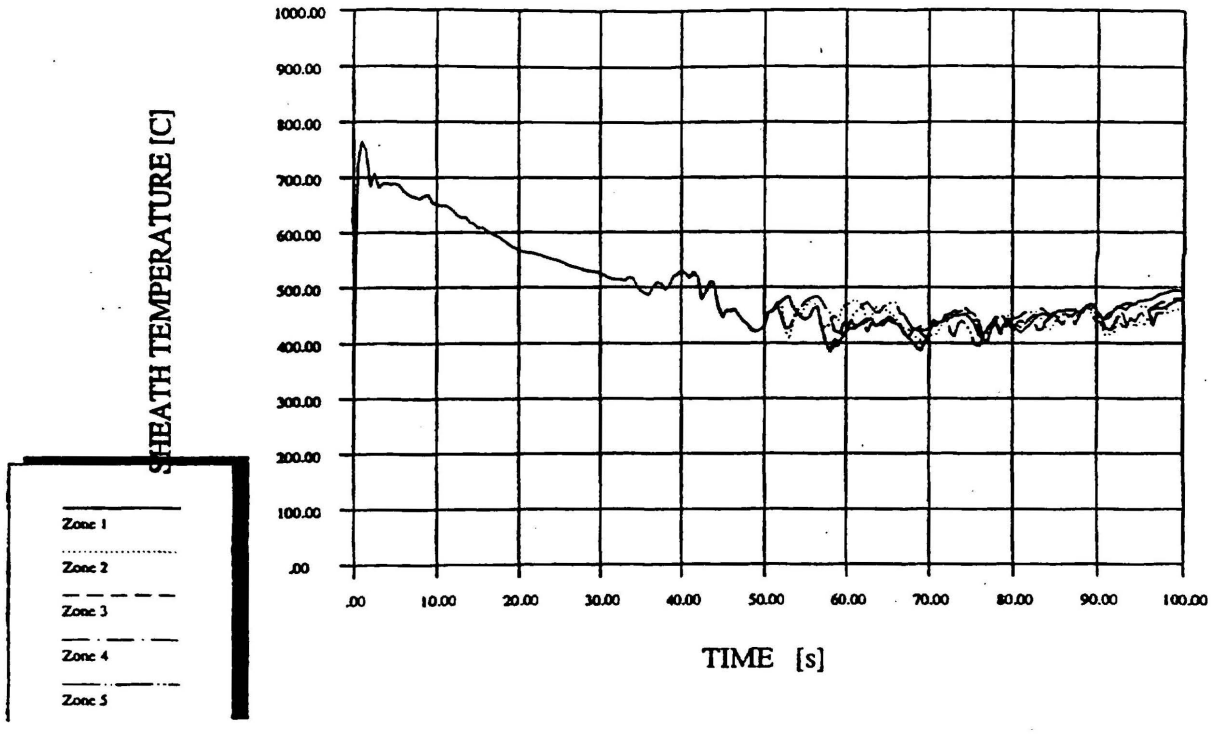

Figure 1. Transient of sheath temperature at the center node of five idential channels in the borken core pass of Bruce A NGS for a 40% RIH break.

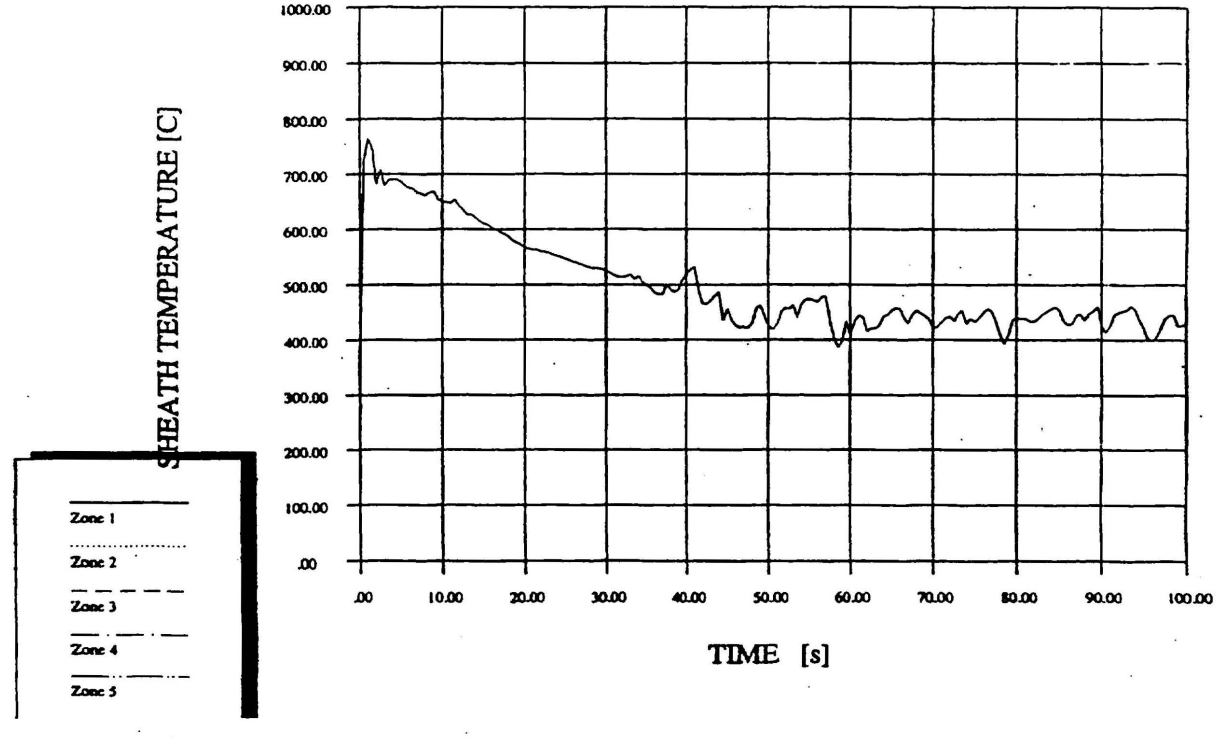

Figure 2. Transient of sheath temperature at the center node of five idential channels in the borken core pass of Bruce A NGS for a 40% RIH break.

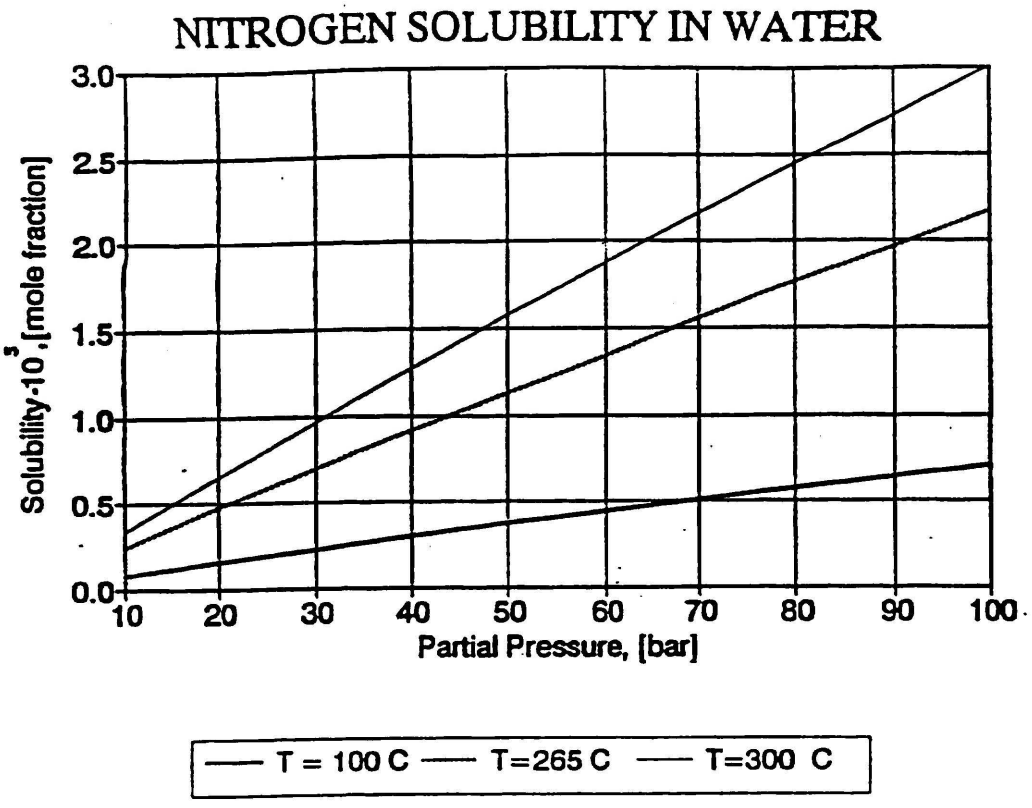

Figure 3. Pressure dependence of the equilibrium concentration of nitrogen in light water.

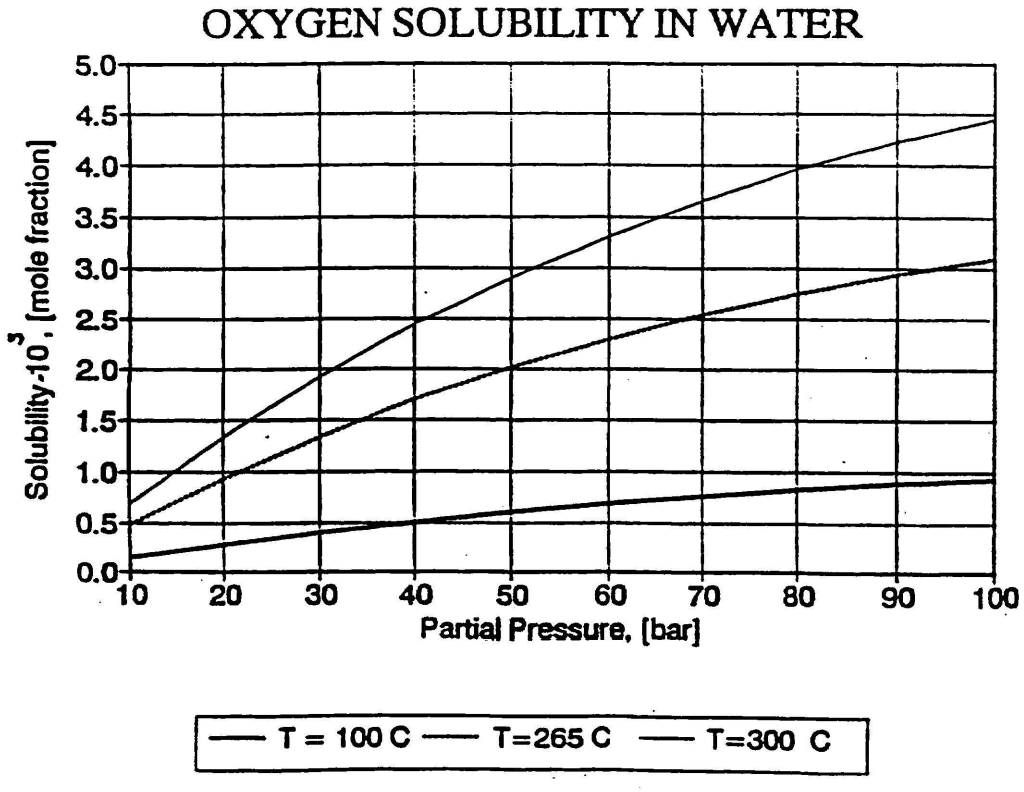

Figure 4. Pressure dependence of the equilibrium concentration of oxygen in light water.

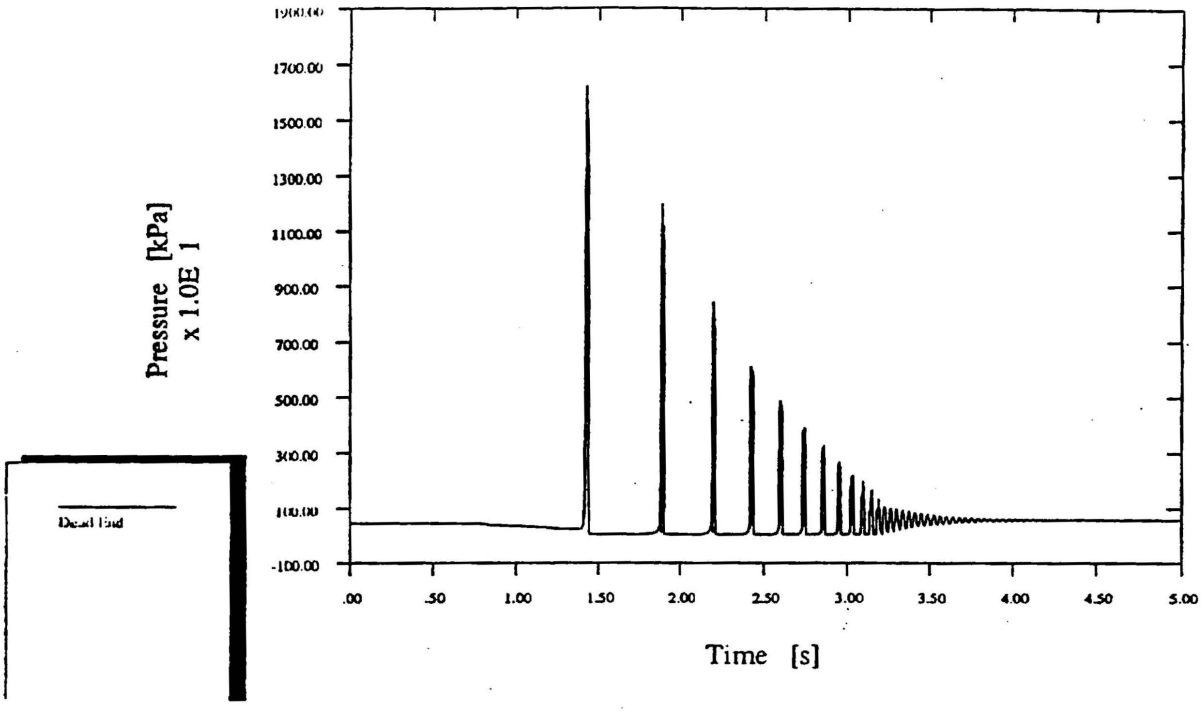

Figure 5. Predicted pressure transient at the dead-end location for Case (1) with tank pressure 654 kPa, water temperature 23 C and steam temperature 150 C.

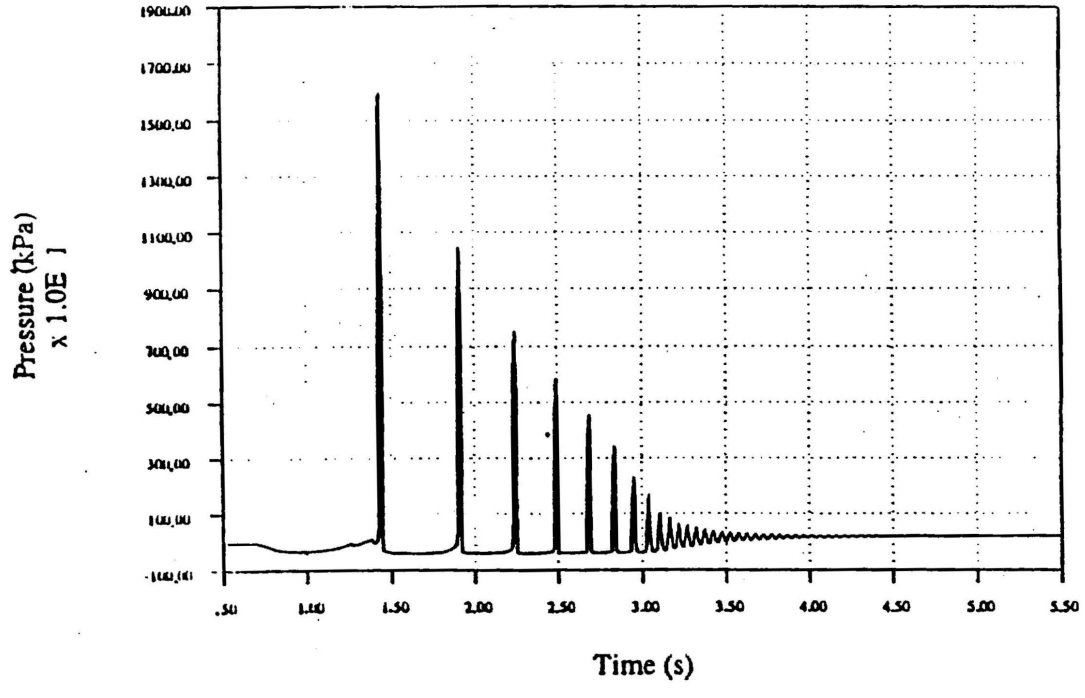

Figure 6. Experimental pressure transient at the dead-end location for Case (1) with tank pressure 654 kPa, water temperature 23 C and steam temperature 150 C.

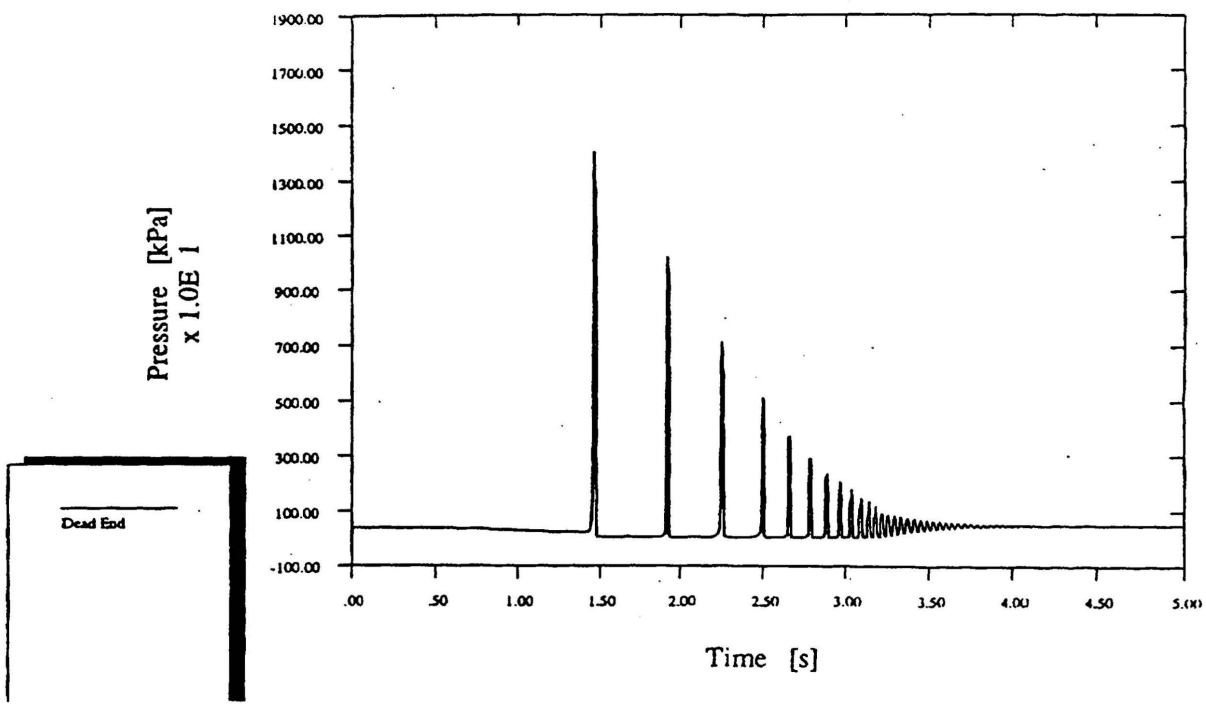

Figure 7. Predicted pressure transient at the dead-end location for Case (2) with tank pressure 551 kPa, water temperature 22 C and steam temperature 142 C.

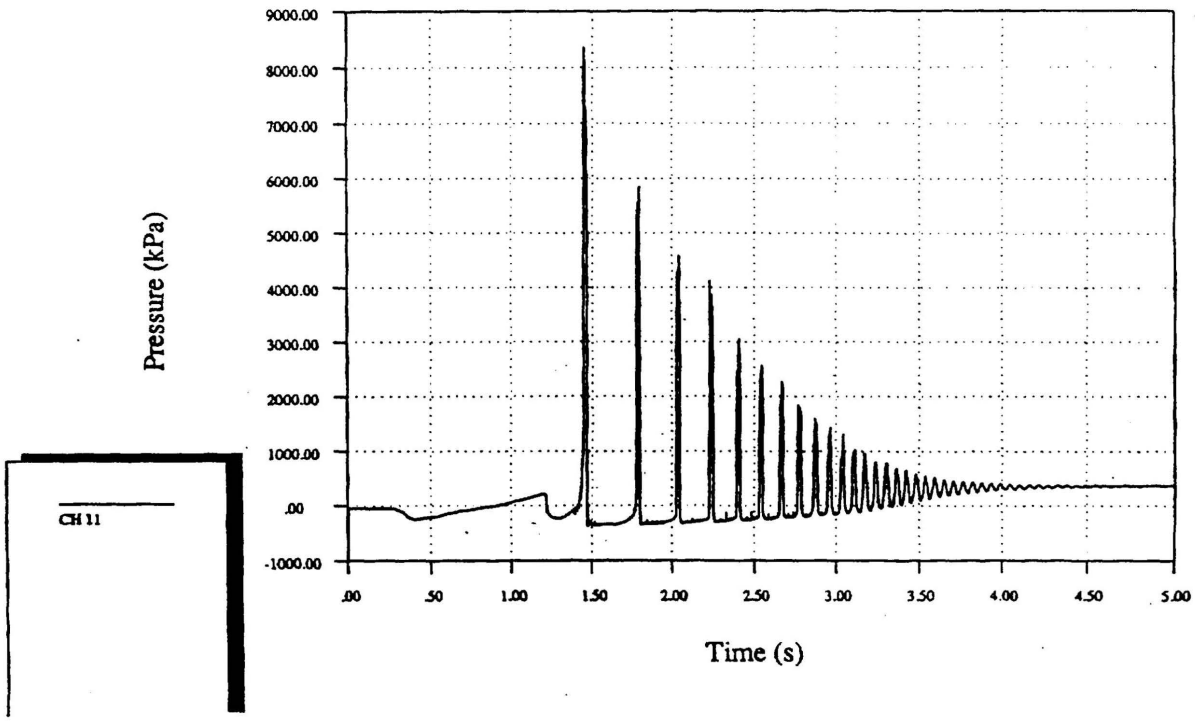

Figure 8. Experimental pressure transient at the dead-end location for Case (2) with tank pressure 551 kPa, water temperature 22 C and steam temperature 142 C.

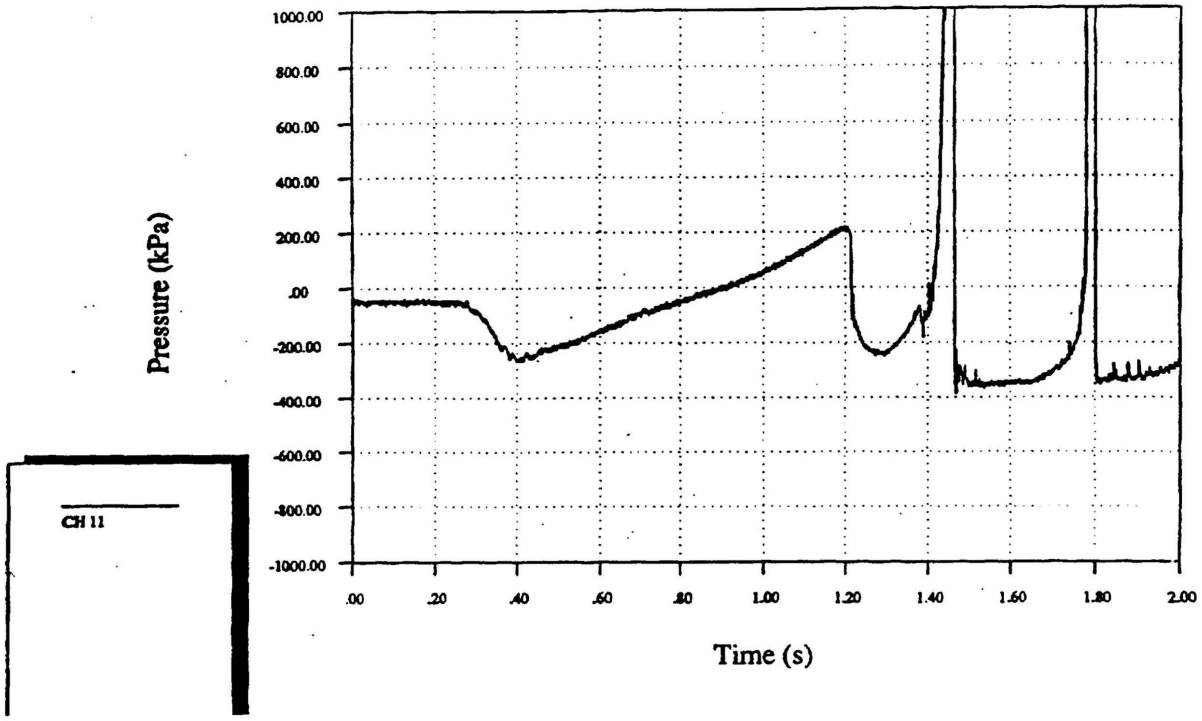

Figure 9. Experimental pressure transient at the dead-end location for Case (2) with tank pressure 551 kPa, water temperature 22 C and steam temperature 142 C.

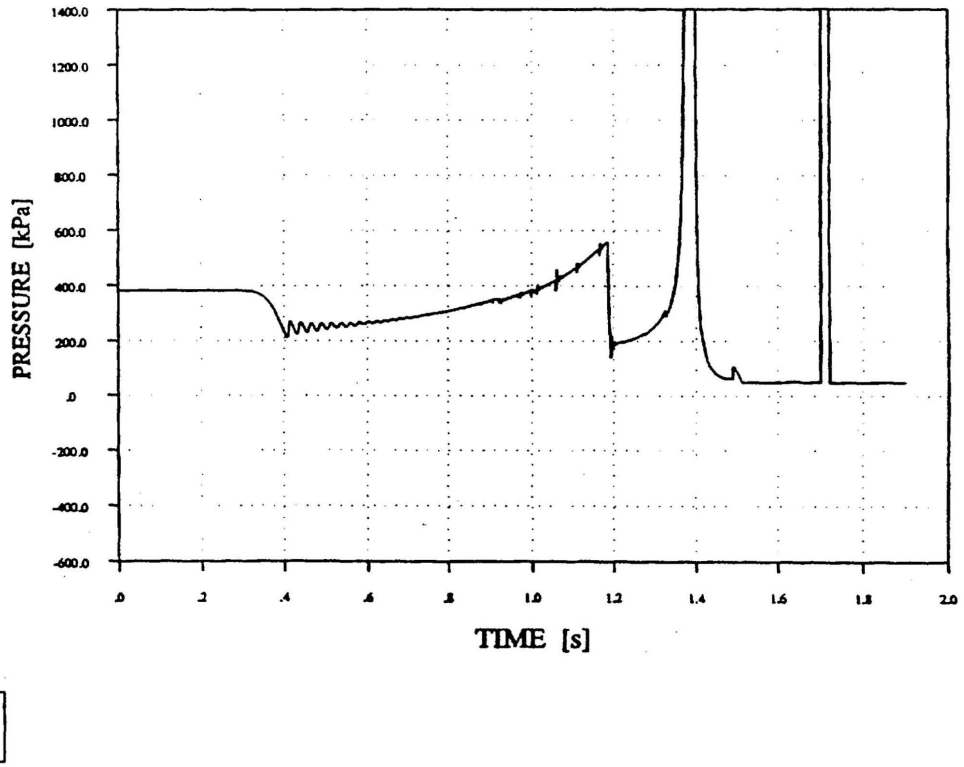

Figure 10. Predicted pressure transient at the dead-end location for Case (2) with tank pressure 551 kPa, water temperature 22 C and steam temperature 142 C.